Two-dimensional correlation functions for density and magnetic field fluctuations in magnetosheath turbulence measured by the Cluster spacecraft

J.-S. He,[1,2] E. Marsch,[2] C.-Y. Tu,[1] Q.-G. Zong,[1,3] S. Yao,[1] and H. Tian[1,4]

[1]   Knowledge of multidimensional correlation functions is crucial for understanding the anisotropy of turbulence. The two-dimensional (2-D) spatial correlation functions (SCFs) obtained in previous studies of space plasma turbulence were restricted to large-length scales and covered a limited angular domain of the two-point separation vector with respect to the mean magnetic field. Here we aim to derive 2-D SCFs with smaller-length scale and nearly full angular distribution for the fluctuations of the number density and magnetic field in magnetosheath turbulence. We use the Cluster four-spacecraft measurements of the fluctuations with respect to a temporally and spatially varying background magnetic field to construct the 2-D SCFs. We find that the correlation function of the density fluctuations shows a pattern similar to that of the magnetic field fluctuations, both of which appear to be composed of two populations, whereby the major population extends along the coordinate parallel to mean magnetic field ($S_{\parallel}$) and the minor one deviates toward the perpendicular coordinate ($S_{\perp}$). This pattern of 2-D SCFs implies that the energy of magnetosheath turbulence seems to cascade, in the inertial range close to the ion scale, mostly transverse to the background magnetic field and meanwhile partly along the field (i.e., $k_{\perp} \gg k_{\parallel}$).

1.   Introduction

[2]   Turbulence in magnetized space plasma has been studied for more than four decades, and gradually its basic as well as detailed characteristics have been revealed, especially for solar wind magnetohydrodynamic turbulence [*Tu and Marsch*, 1995; *Goldstein et al.*, 1995; *Bruno and Carbone*, 2005]. However, there still remain a lot of unsolved problems and issues, one of which is the nature and origin of the anisotropy of turbulent fluctuations in k vector space. An alternative to the description of turbulence by an energy spectrum in Fourier space is the description in real space by a multidimensional spatial correlation function (SCF), which can more easily be derived from the *in situ* measurements than a multidimensional power spectral density (PSD). The two-dimensional (2-D) SCF corresponding to large-scale solar wind turbulence was firstly presented by

Matthaeus et al. [1990], who used multiple data sets from a single spacecraft. The lower limit of the separation distance (vector **S** with the longitudinal, $S_{\parallel}$, and transverse, $S_{\perp}$, component with respect to the mean field) considered in that paper was 10^5 km, which is 3 orders of magnitude larger than that of the typical ion gyroradius (ρ_i) in the solar wind. The correlation length of solar wind turbulence was estimated based on cross-correlation analysis of simultaneous two-point measurements [*Matthaeus et al.*, 2005; *Weygand et al.*, 2009]. Recently, *Osman and Horbury* [2007] used Cluster four-spacecraft data to estimate the 2-D SCF of solar wind turbulence, with the lower limit of the separation distance (**S**) being 2×10^3 km (~20 ρ_i). However, the spatial extent of that correlation function is far from a full coverage of the 2-D **S** space. To present such a 2-D SCF with a nearly full angular distribution and more complete coverage of the separation distances down to $5\rho_i$ is the main objective of this paper. Besides the SCF derived in this article, second-order structure function obtained by using the four-satellite technique is another way of studying the wave vector anisotropy of turbulence [*Chen et al.*, 2010]. They revealed that the second-order structure functions for both perpendicular and parallel fluctuations between ion and electron scales are anisotropic, with the values at large angles to magnetic field being greater than smaller angles.

[3]   To obtain such a comprehensive correlation function for solar wind turbulence, the time range of the data required

[1]Department of Geophysics, School of Earth and Space Sciences, Peking University, Beijing, China.
[2]Max-Planck Institute for Solar System Research, Katlenburg-Lindau, Germany.
[3]Center for Atmospheric Research, University of Massachusetts Lowell, Lowell, Massachusetts, USA.
[4]Now at National Center for Atmospheric Research, Boulder, Colorado, USA.

must be long enough to cover a wide distance range and to include various angles of the solar wind velocity with respect to the mean magnetic field (θ_{VB}). However, the Cluster satellites can only stay in the continuously undisturbed solar wind for quite a short time, and thus are not able to meet this requirement. In contrast, the Cluster measurements made in the magnetosheath can cover a wider range of θ_{VB}. Therefore, we chose the magnetosheath turbulence as our target. However, magnetosheath turbulence is more complicated than solar wind turbulence [see *Alexandrova*, 2008, and references therein]. In the magnetosheath, Alfvén-Ion cyclotron (AIC) and mirror-mode waves may be excited by linear instability due to the dominant ion temperature anisotropy (with $T_\perp > T_\parallel$) [*Schwartz et al.*, 1996; *Lucek et al.*, 2005]. These modes, if they exist, should result in prominent spectral peaks at low frequencies. Their wave vector features were already investigated [e.g., *Narita and Glassmeier*, 2006]. A mirror-mode-like cascade was inferred by *Sahraoui et al.* [2006], on the basis of fluctuations with zero frequency in the plasma frame and a dominant perpendicular wave vector ($k_\perp$). *Mangeney et al.* [2006] studied, using Cluster C1 spacecraft measurements, the 1-D reduced PSD of magnetic field fluctuations on the electron scales and found it to be strongly anisotropic, with most energy residing at an angle θ_{VB} around 90°. This kind of 1-D reduced PSD was found to become concentrated around $\theta_{\mathrm{VB}} \sim 90°$, when the spacecraft frame frequency exceeded the ion cyclotron frequency [*Alexandrova et al.*, 2008]. Their results imply the $k_\perp \gg k_\parallel$ wave vector anisotropy [*Leamon et al.*, 1998; *Horbury et al.*, 2008]. However, the 2-D PSD (or its inverse Fourier transform, the 2-D SCF) of the magnetosheath turbulence has not yet been established. Below we will show that, the wave vector anisotropy previously found in 1-D reduced PSDs is again consistent with our findings of the anisotropy of 2-D SCF.

[4] Compressive fluctuations, e.g., magnetic field strength and density fluctuations, are another important component of turbulence besides transverse magnetic field fluctuations. Their energy cascades are theoretically predicted to be a kind of passive scalar turbulence [*Goldstein et al.*, 1995], both at the inertial and dissipation scales, due to their nonlinear interactions, e.g., with kinetic Alfvén waves [*Schekochihin et al.*, 2009]. Parallel magnetic field fluctuations $\delta B_\parallel^2$ in the magnetosheath, one kind of compressive fluctuations, were found to have larger PSD for large θ_{VB} than that for small θ_{VB} (the index to $k_\perp \gg k_\parallel$ wave vector anisotropy) [*Alexandrova et al.*, 2008]. *Marsch and Tu* [1990] found that, in the inner heliosphere, the density spectra below 10^{-2} Hz for the low-speed and high-density flows come close to a $-5/3$ spectral law supporting the concept of a passive modulation of the density by Alfvénic fluctuations, while the density spectra for the high-speed and low-density flows reveal a flatter high-frequency part, and there do not obey the $-5/3$ power law. Rapid fluctuation of electron density up to 2.5 Hz in the solar wind has been studied by *Kellogg and Horbury* [2005], who also reported a similar flattering of the lowest-density spectra. According to our knowledge, the wave vector anisotropy of density fluctuations in the magnetosheath turbulence has not yet been addressed.

[5] In this article, we present 2-D SCFs of density and magnetic field fluctuations in the magnetosheath by employing the method proposed by *Horbury* [2000] and *Osman and Horbury* [2007] to the Cluster FGM and EFW data sets. We find that both of the 2-D SCFs show a two-population structure, like the "Maltese cross" introduced by *Matthaeus et al.* [1990]. According to Figure 3 of *Matthaeus et al.* [1990], the quasi-2-D population becomes noticeable in the 2-D SCF for large parallel scales ($S_\parallel > 1500$ Mm$\sim 15 \times 10^3 \rho_i$). Here in our case, the scale of appearance of quasi-2-D population extends down to $5\rho_i$. This result indicates a composition of the PSD by two populations for the magnetosheath turbulence, within a k range of $[1/70, 1/5] \rho_i^{-1}$, where the perpendicular PSD population dominates over the parallel one (i.e., $k_\perp \gg k_\parallel$).

2. Data Analysis of Cluster Measurements

2.1. Overview of Cluster Measurements in the Magnetosheath

[6] The data sets used here were obtained from measurements by the FGM [*Balogh et al.*, 2001], EFW [*Gustafsson et al.*, 2001], and CIS [*Rème et al.*, 2001] instruments aboard Cluster [*Escoubet et al.*, 2001] and correspond to the period from 0000 to 0600 UT on 19 December 2001, when Cluster stayed in the magnetosheath. The magnetosheath turbulence on this day was already studied by *Mangeney et al.* [2006] and *Alexandrova et al.* [2008], however their study was limited to its θ_{VB} variation of 1-D reduced PSDs of magnetic field fluctuations. Figure 1 shows an overview of the Cluster C1 measurements made during this time. The time variation of the three magnetic field components (B_x, B_y, B_z in the GSE coordinate system) with a spacecraft spin resolution of 4 s is illustrated in Figure 1a. The bulk flow velocity components in the GSE coordinate system are displayed in Figure 1c, and the angles between the velocity and magnetic field vectors (θ_{VB}) are shown in Figure 1d, which reveals a wide range of variations. The ion number density variation, as measured by HIA on CIS with a time resolution of 4 s, is plotted as the black line in Figure 1b. The red line in Figure 1b represents the electron number density, which was derived from the EFW probe spacecraft potential in calibration with the HIA ion number density. According to *Pedersen et al.* [2008], the connection between electron densities and EFW potentials can be established by calibrating them with the electron densities from WHISPER [*Décréau et al.*, 1997] or ion densities from CIS/HIA, both of which are in good agreement in the solar wind and magnetosheath. We do not have the electron densities from WHISPER, which may be due to the absence of Langmuir waves there. Therefore, the HIA ion densities are used as a benchmark for calibration. From Figure 1b, we can infer consistency between the ion and electron number densities.

2.2. Mapping of Temporal Cross Correlations Onto Coordinate Space

[7] The Cluster four-spacecraft measurements are advantageous over a single-spacecraft measurement in analyzing, with varying separation vectors, the spatial correlations between field variables, since Cluster measurements can produce six time-cross-correlation series in a given time interval, and each series contains different separation distances and various unit separation vectors. Following
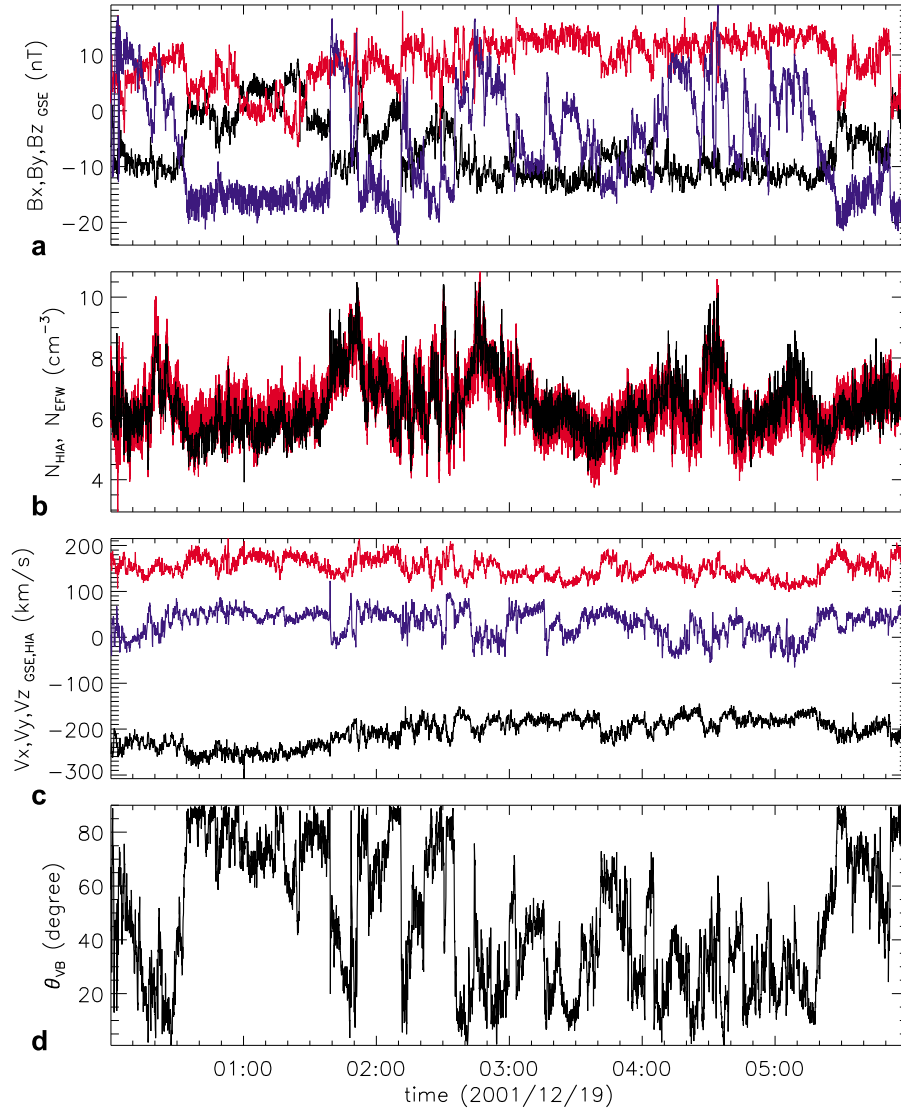
Figure 1. Overview of Cluster C1 measurements in the magnetosheath during the interval [0000, 0600] UT on 19 December 2001. (a) Time variations of B_x (black), B_y (red), and B_z (blue) components in GSE coordinates measured by FGM. (b) Time variations of N_i (black) and N_e (red) measured by CIS/HIA and EFW, respectively. (c) Time profiles of flow velocity components, V_x (black), V_y (red), and V_z (blue) in GSE measured by CIS. (d) Time variations of θ_{VB} between $\mathbf{B}$ and $\mathbf{V}$.

Osman and Horbury [2007], we rewrite the cross correlation of the fluctuations (e.g., $\delta B_\perp$) measured by ith and jth spacecraft over a time interval T as $R_{\delta B_\perp}{}^{i,j}(\tau)$, where $\tau(=t_j - t_i)$ denotes the time lag τ of the sampling by the jth spacecraft with respect to the sampling by the ith spacecraft. The separation vector $\mathbf{S}$ corresponding to τ is given by the relation, $\mathbf{S} = \mathbf{r}_{i,j} - \mathbf{V}_{flow}\tau$, where $\mathbf{r}_{i,j}(=\mathbf{r}_j - \mathbf{r}_i)$ is the separation vector between the positions of the jth and ith spacecraft, and $\mathbf{V}_{flow}$ is the plasma bulk flow velocity vector. Similar to *Osman and Horbury* [2007], we removed all the time lags which yield $|V_A \tau|/|\mathbf{r}_{i,j} - \mathbf{V}_{flow}\tau| > 0.2$, and thus are expected to break Taylor's hypothesis, which we wanted to avoid. Taylor's hypothesis is usually not valid for analyzing spatial correlation based on the measurements from only one satellite in the magnetosheath, especially in the subsolar region. However, when we estimate the spatial correlation based on the measurements at multiple separated positions,

the validity still holds under certain condition we described above, which means that the separation distance of fluctuations is much larger than the wave traveling distance and thus avoids the influence of wave temporal fluctuations on the spatial correlation. In our case, the Cluster 4 satellites were in the flank of magnetosheath rather than the subsolar region, where the average flow velocity is about 273 km/s more than twice of local Alfvén speed (123 km/s). For every τ satisfying the Taylor's hypothesis, we rewrite $R_{\delta B_\perp}{}^{i,j}(\tau)$ as $R_{\delta B_\perp}{}^{i,j}(\mathbf{S})$. $\mathbf{S}$ can be expressed as $S_\parallel \hat{r}_\parallel + S_\perp \hat{r}_\perp$ with $\hat{r}_\parallel$ and $\hat{r}_\perp$ being unit vectors parallel and perpendicular to the mean magnetic field. Therefore, we have $R_{\delta B_\perp}{}^{i,j}(S_\parallel, S_\perp)$, which is a projection result of temporal cross correlation onto the 2-D coordinate space.

[8] In Figure 2, we show an example of mapping temporal cross correlations onto the coordinate space. The relevant time range [0222:29, 0232:29] UT is marked by a blue
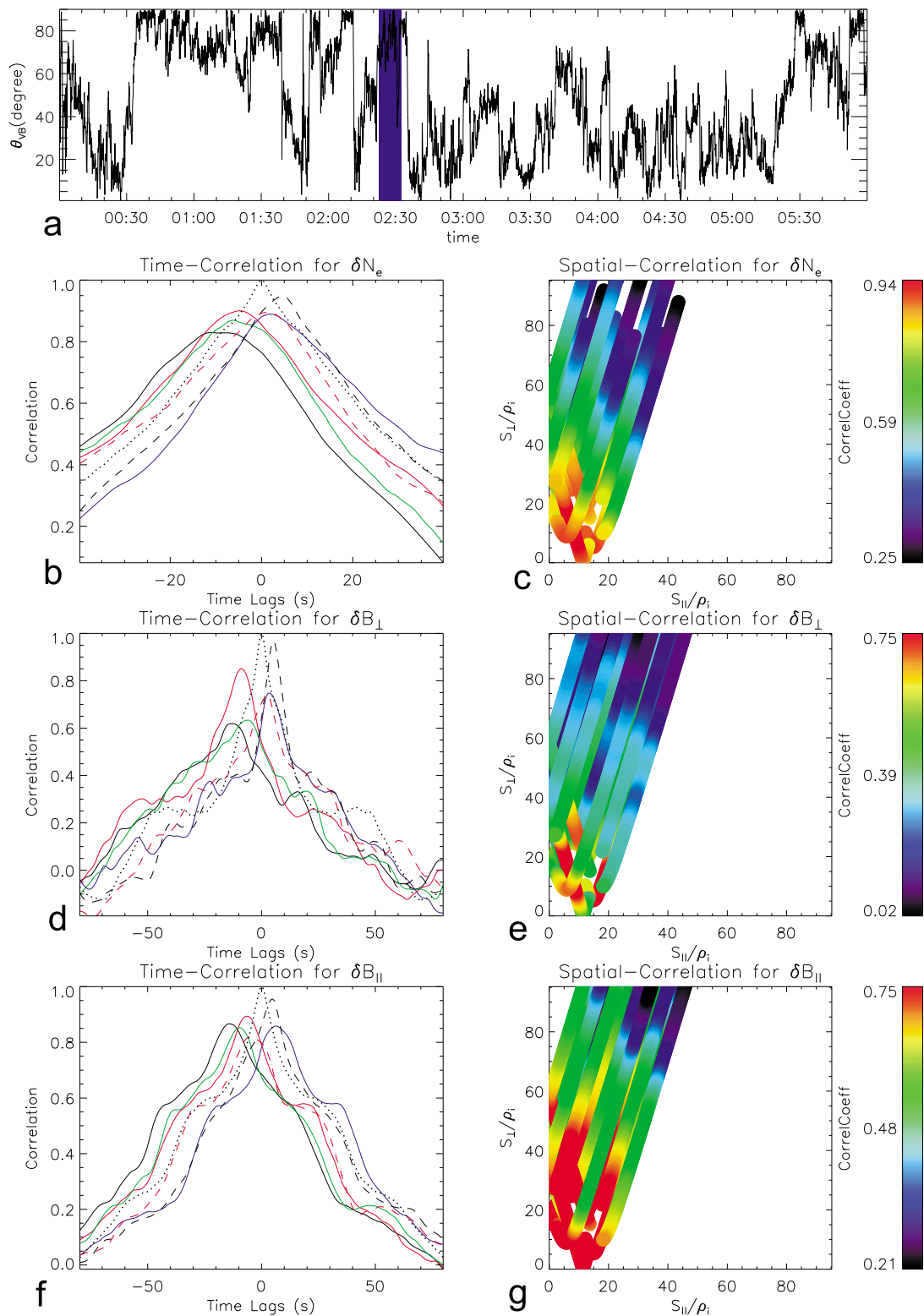
Figure 2. An example of projecting the temporal cross correlation onto the 2-D **S** space. (a) The selected time interval [0222:29, 0232:29] UT marked by a blue shadow. (b) Six temporal cross correlations of δN_e (black solid, red solid, green solid, blue solid, black dashed, and red dashed for C1-C2, C1-C3, C1-C4, C2-C3, C2-C4, and C3-C4, respectively) and one autocorrelation of C1 measurements (black dotted). (c) Projection of the six temporal cross correlations of δN_e onto the 2-D **S** space by using the method described in section 2.2. (d) Temporal cross correlations and autocorrelation of $\delta B_\perp$, with the line styles having the same meaning as in Figure 2b. (e) Projection of the six temporal cross correlations of $\delta B_\perp$ onto the 2-D **S** plane. (f and g) The case for $\delta B_\parallel$.
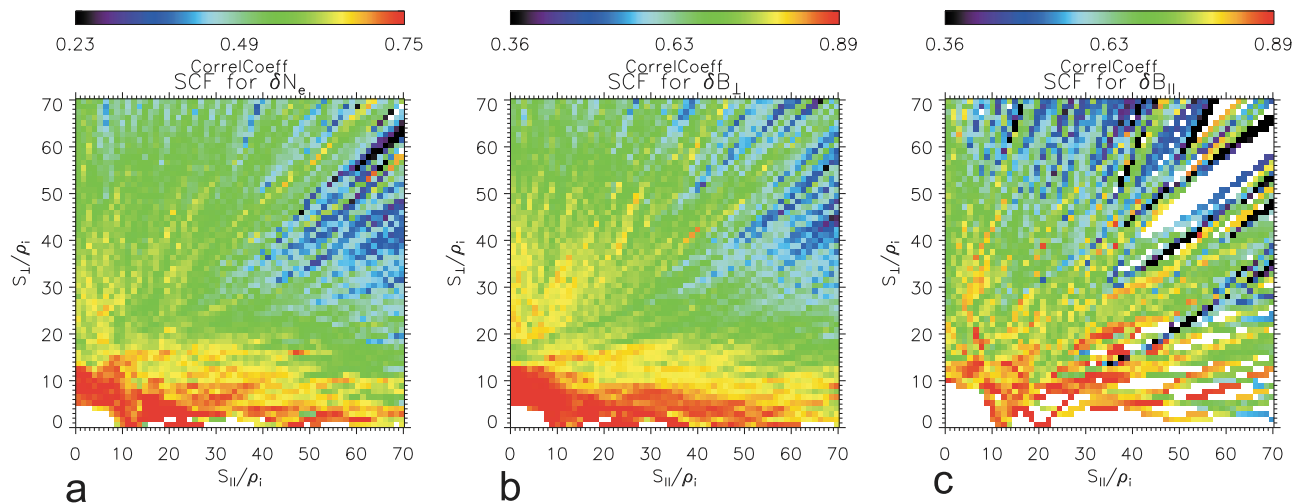
Figure 3. Two-dimensional spatial correlation functions (SCFs) for (a) δN_e, (b) $\delta B_\perp$, and (c) $\delta B_\parallel$. The derivation of them is described in section 2.3.

shadow in Figure 2a, corresponding to a time interval T of 10 minutes. The angle θ_{VB} usually does not change a lot during 10 minutes. If we set a longer time interval, e.g. 30 minutes, θ_{VB} will vary in a wide range during the 30 minutes (see Figure 2a). If we shorten the time interval to a smaller value, saying 1 minute, then few correlation times will be included and the correlation result may be not reliable. The correlation time is estimated to be about 0.5 minute according to the formula $T_C = \int_0^{R(\tau) \to 0} R(\tau)/R(0)d\tau$ as applied to the correlation profiles in Figure 2, where τ is the time lag and R is the correlation coefficient. The temporal cross correlations between different pairs of density fluctuations (δN_e) are displayed in Figure 2b, and they are projected onto the coordinate space (2-D S space) in Figure 2c. The abscissa ($S_\parallel$) and ordinate ($S_\perp$) in Figure 2c are plotted in unit of ρ_i, which is ~105 km in this case. The separation distance between two different satellites is around 2000 km. Figures 2d and 2e show the mapping of the temporal cross correlations for $\delta B_\perp$ onto the 2-D S space. $\delta B_\perp$ is defined as $\delta \boldsymbol{B} \cdot (\hat{b} \times \hat{x})$, where $\hat{b}$ is the unit vector of local mean magnetic field and $\hat{x}$ is the unit vector of x axis of GSE coordinates. We assume that $\delta B_\perp$ is rotational symmetric about local mean magnetic field. This definition of $\delta B_\perp$ is used hereafter. It can be inferred that, in this time interval, the δN_e as well as $\delta B_\perp$ sequences measured by the four Cluster spacecraft are similar and apparently highly cross correlated, since the six temporal cross-correlation profiles resemble the temporal autocorrelation profiles (black dotted lines in Figures 2b and 2d).

[9] We note a spacecraft spin effect in the δN_e time series, which originates from the asymmetric plasma distribution around the satellite caused by wake effects or photoelectrons [*Pedersen et al.*, 2008], and which must be eliminated before making a temporal correlation. Otherwise, an artificial periodic oscillation would be added on the profile of the correlation coefficient. Such artificial periodic oscillation cannot be completely removed by applying a multinotch filter to the δN_e time series, since the residual spin harmonic spikes of the related PSD would still remain, however we

modify the filter. Alternatively, we find that the running-averaged δN_e with a time width of 2 s leads to a correlation-coefficient profile which gives the same trend as the original one without artificial oscillations, and which therefore is adopted for our study. We resampled the $\delta B_\perp$ time series, with an original sampling rate of 22/s, to create a new one of 5/s, in order to be consistent with that of the δN_e time series. We note that the aliasing in frequency domain caused by downsampling does not affect significantly the corresponding PSD probably due to the power law shape of PSD, which means that the downsampled time profiles can still be used without suppressing the aliasing effect.

2.3. Establishment of 2-D Spatial Correlation Functions and Their Reliability

[10] For other time intervals different from that in Figure 2, there are many more θ_{VB} values, corresponding to different profiles of the correlation coefficient. Over the duration of 6 h, we apply a running window with a time interval T of 10 min and a time step ΔT of 2.5 min, to get a set of correlation-coefficient profiles with a wide range of θ_{VB}. We select out those time ranges when the maximum values of the six correlation-coefficient profiles are all larger than 0.6, and then project the chosen temporal cross correlations onto the 2-D S plane. The correlation threshold of 0.6 is selected after practical experiences. We find that, when all the six cross-correlation profiles have maximum correlation coefficients (R_m) larger than 0.6, they appear similar to each other with some shift of time lags, which indicates a nice cross correlation between the four satellite measurements. For the other time intervals with $R_m < 0.6$, the correlation profiles deviate a lot from each other, which implies the unreliability of the cross-correlation results. This 2-D S plane is divided into many square cells with a size of 1.2×1.2 in units of ρ_i. The spatial correlation coefficient of every square cell is thus assigned to an average of the correlation coefficients corresponding to it. In this way, 2-D the spatial correlation function (SCF) is obtained. The resulting 2-D SCFs for δN_e, $\delta B_\perp$, and $\delta B_\parallel$ are illustrated in Figures 3a, 3b, and 3c. The scale length revealed by the SCFs ranges between 5 ρ_i and 70 ρ_i. It is interesting to find

that the δN_e SCF shows a structure similar to that of the $\delta B_\perp$ SCF. From Figure 3, we find that the contour of higher correlation (in red) is extending along $S_\parallel$, while the contour of intermediate correlation (in yellow and green) is extending in various directions mainly with angles to $S_\perp$ being less than 45°. Therefore, the major population of the correlation function comes from the contours along $S_\parallel$, and the minor population from the fan-like contours deviating toward $S_\perp$. However, the SCF for $\delta B_\parallel$ is not as fully filled as that for δN_e, and some difference appears between them. In theory, both the $\delta B_\parallel$ and δN_e represent the compressibility of magnetized plasma. For the compressional wave propagating at a certain angle with respect to background magnetic field (θ_{kB}), the enhancement of either magnitude is expected to be accompanied with an increase of the other one. However, the compressibility ratio between the PSD of $\delta B_\parallel$ and δN_e varies when the compressional wave propagates at different θ_{kB}. This variation of the compressibility ratio might result in the pattern difference between $\delta B_\parallel$ PSD and δN_e PSD, and likewise $\delta B_\parallel$ SCF and δN_e SCF. It is still unknown why the pattern of $\delta B_\perp$ SCF looks similar to that of δN_e SCF.

[11] We note that it is difficult to estimate the parallel and perpendicular correlation lengths ($\lambda_\parallel$ and $\lambda_\perp$) for both the major and minor populations of the SCF by using an assumed multivariate nonlinear fitting function $SCF(S_\parallel, S_\perp) = \alpha \cdot \exp(-S_\parallel/\lambda_{\parallel 1} - S_\perp/\lambda_{\perp 1}) + (1 - \alpha) \cdot \exp(-S_\parallel/\lambda_{\parallel 2} - S_\perp/\lambda_{\perp 2})$, where the parameters ($\alpha$, $\lambda_{\parallel 1}$, $\lambda_{\perp 1}$, $\lambda_{\parallel 2}$, $\lambda_{\perp 2}$) to be fitted represent the energy fraction of major population, the parallel and perpendicular correlation lengths for major and minor populations, respectively. It is also difficult to define $\lambda_\parallel$ and $\lambda_\perp$ as the width at a correlation level of $\exp(-1) \sim 0.36$, since the SCFs obtained in this data analysis do not have a complete coverage in the coordinate space, as the coordinates extend beyond 70 ρ_i and the correlation coefficients approach to lower correlation levels. As an alternative, the correlation length is assigned to the width at a relatively higher correlation level. The major population of the observed SCF structures is thus estimated to have a parallel correlation length around 60 ion Larmor radii and a perpendicular correlation length around 10 ion Larmor radii, if we define the correlation length to be the width at a correlation level of 0.65 for δN_e SCF and 0.75 for $\delta B_\perp$ SCF. The lower correlation level for δN_e SCF than that of $\delta B_\perp$ SCF might be due to a partial decorrelation of density fluctuations, which is transformed from the electric potential with certain uncertainty.

[12] Next we need to check whether our method, yielding these two maps of the mean correlation-coefficient distribution, is reliable in describing the 2-D SCFs of magnetosheath turbulence. According to *Matthaeus et al.* [1986], turbulence can be considered as weakly stationary if its correlation function is independent of the start point in time, and if the fluctuations are nearly ergodic, which is the case given the time duration is long enough, say much larger than the correlation time. Therefore, in our study the selected time series of δN_e and $\delta B_\perp$ can be regarded as weakly stationary and almost ergodic, since the correlation-coefficient profiles change little when the start time is shifted somewhat (but by less than 2 min to guarantee a similar θ_{VB}), and as the chosen time interval T (10 minute) is much longer than the correlation time (~0.5 minute). Moreover, the magnetosheath downstream tends to be almost stationary during

6 h, within which the solar wind upstream usually remains in a steady state.

[13] Figure 4 demonstrates the reliability of our suggestion to regard the distribution of correlation-coefficient averaged in every cell as being representative of the real 2-D SCF. Figures 4a and 4b illustrate the estimated standard deviation σ and the number of counts (n) of correlation coefficients falling in each cell for δN_e. Figure 4c shows the confidence interval CI for the mean correlation coefficient in every cell, which is calculated by means of the formula $CI = 2 \cdot t_{C,n} \cdot \sigma/\sqrt{n}$, with $t_{C,n}$ being the upper $(1 - C)/2$ critical value for the t distribution with $n - 1$ degrees of freedom. The confidence level C adopted here is 95%. The smaller CI is the more credible is the average correlation coefficient. We can therefore have trust in our SCFs shown in Figure 3, since most parts of CI (<0.25) are smaller than the minimum value of the SCFs. Figures 4d, 4e, and 4f shows the reliability of $\delta B_\perp$ SCF.

[14] To see how the PSD of the fluctuations of number density and magnetic field change along with θ_{VB}, we estimate the slopes of PSD in both the lower and higher frequencies for different θ_{VB} and plot them in Figure 5. The different points (θ_{VB}, slope) in Figures 5b, 5c, 5e, and 5f correspond to fluctuations measured by Cluster C1 in different time ranges, which were selected in section 2.3, with all of the six cross-correlation profiles in that time range having maximum values exceeding 0.6. For the fluctuations measured by the other three satellites, they show similar results. The PSD of density fluctuations (Figure 5a) shows an enhancement just below the spectral break (at ~0.6–0.7 Hz). The PSD of $\delta B_\parallel$ in the same time range also has a bump at the same frequency. The bump in both PSD of δN_e and $\delta B_\parallel$ may be interpreted as a signature of mirror mode [*Schwartz et al.*, 1996; *Sahraoui et al.*, 2006] which has a wave vector anisotropy with $k_\perp \gg k_\parallel$, as inferred from the observed SCFs. Figure 5d illustrates the PSD of $\delta B_\perp$. There is a small bump around the spectral break (0.1–0.2 Hz), which may be related to the presence of Alfvén vortices [*Alexandrova et al.*, 2006]. The magnetic structures associated with Alfvén vortices are like field-aligned current tubes, which cause the magnetic field disturbances to have the wave vector anisotropy (i.e., $k_\perp \gg k_\parallel$). This anisotropy is again consistent with the anisotropic SCFs presented here. We find that there are rising trends of spectral indices with θ_{VB} for both $PSD(\delta N_e)$ and $PSD(\delta B_\perp)$ in the high-frequency segments beyond 0.1 Hz in the spacecraft frame. The increase of the spectral index with increasing θ_{VB} was also reported by *Horbury et al.* [2008] and *Podesta* [2009] in the solar wind turbulence, which may shed light on the required turbulence model.

3. Summary and Discussion

[15] We have presented the 2-D spatial correlation functions for the compressive and transverse turbulent fluctuations, δN_e and $\delta B_\perp$, in the magnetosheath of the Earth's magnetosphere. It is interesting to find that both of these two SCFs with a scale length range of [5,70] ρ_i show similar structures, which have a major population extending along $S_\parallel$ and a fan-like minor population deviating toward $S_\perp$. Based on this structure of SCF, one can infer that the corresponding 2-D PSD may also consist of two populations,
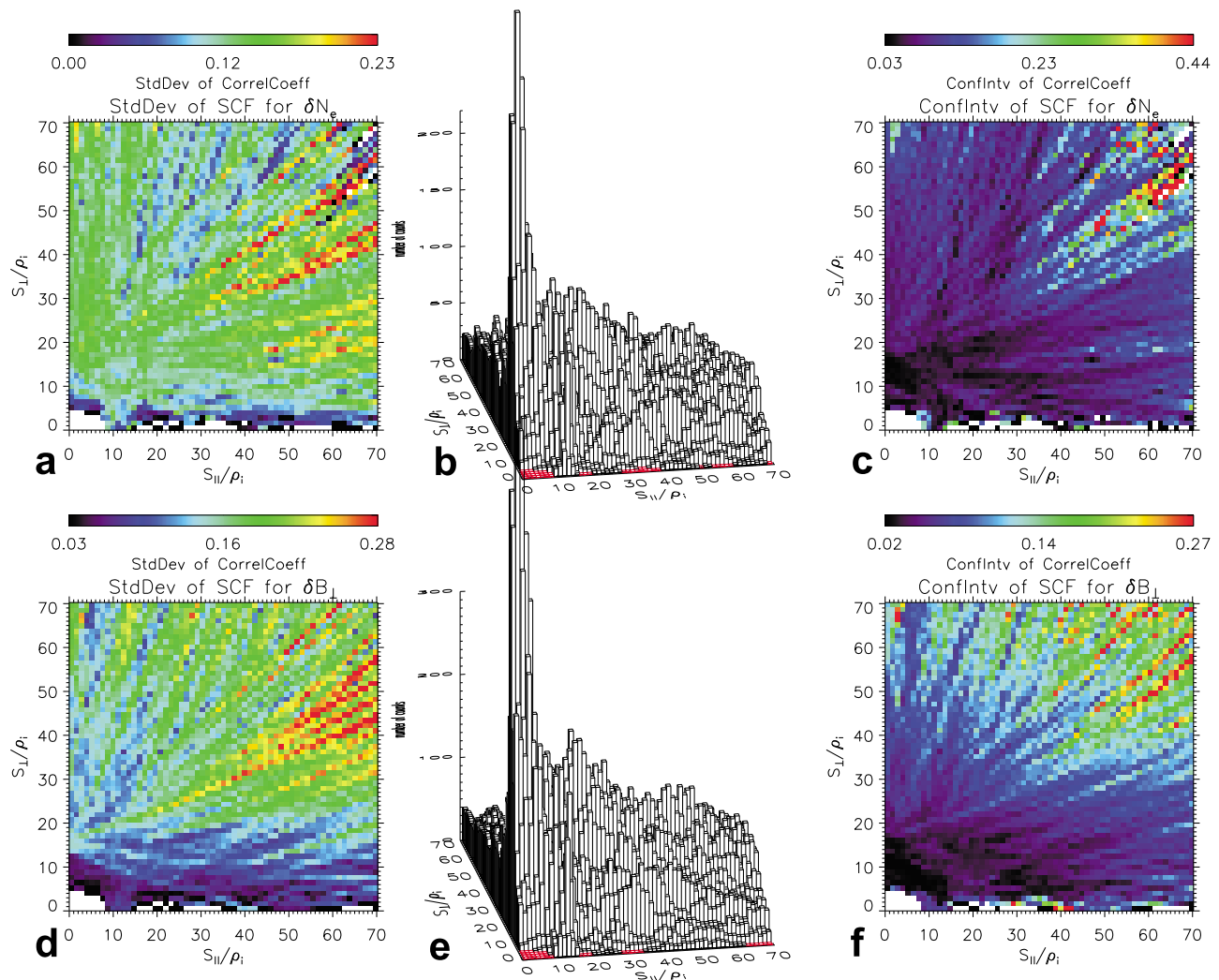
Figure 4. Credibility estimation of the 2-D SCFs for (a, b, and c) δN_e and (d, e, and f) $\delta B_\perp$. Distribution of the estimated standard deviation for the correlation coefficient in every square cell (Figures 4a and 4d). Histograms of the number count in every square cell (Figures 4b and 4e). The cells in red represent the zero number count. Distribution of the confidence interval for the estimated mean correlation coefficient in every square cell (Figures 4c and 4f). The related confidence level is 95%.

with the major being in the $k_\perp$ direction and the minor close to the $k_\parallel$ direction. We note that in practice a high-quality 2-D PSD cannot be derived from a direct Fourier transformation of the 2-D SCF, for the reason that many parts of the 2-D PSD would turn out to be negative, even though the 2-D SCF was smoothed. A new method is needed for the reconstruction of 2-D PSD in the future. Nevertheless, our findings about the dominance of parallel population in SCF ($S_\parallel \gg S_\perp$) indicate the dominance of perpendicular population in multidimensional PSD ($k_\perp \gg k_\parallel$). This indication is consistent with the wave vector anisotropy of magnetosheath turbulent fluctuations as revealed from θ_{VB} variation of 1-D reduced PSD in previous studies [e.g., *Mangeney et al.*, 2006; *Alexandrova et al.*, 2008].

[16] Theoretical prediction based on only one singe wave mode cannot cover the whole of what we have observed. The mixture of various modes (e.g., Alfvén (cyclotron) waves and mirror modes) and structures (e.g., Alfvén vor-

tices and pressure-balanced structures) may be responsible for the complexity of observations. It appears that according to our findings there might be two paths of energy transfer: the major cascade is in the direction nearly perpendicular to the local mean magnetic field, while the minor cascade is parallel. But the wave nature underlying this anisotropic turbulence cascade remains unclear. We may speculate whether critical balance cascading of Alfvén waves [*Goldreich and Sridhar*, 1995] or cascading of pressure-balanced structures (e.g., perpendicular slow magnetoacoustic waves [*Mangeney et al.*, 2006] or mirror modes [*Sahraoui et al.*, 2006]) may be responsible for the SCF population parallel to $S_\parallel$, and if the cascading of parallel Alfvén waves (Alfvén-Ion cyclotron waves at high frequencies) may contribute to the SCF population lying close to $S_\perp$. All these three kinds of wave mode if with oblique wave vectors are theoretically predicted to be responsible for the anticorrelation between electron density and magnetic
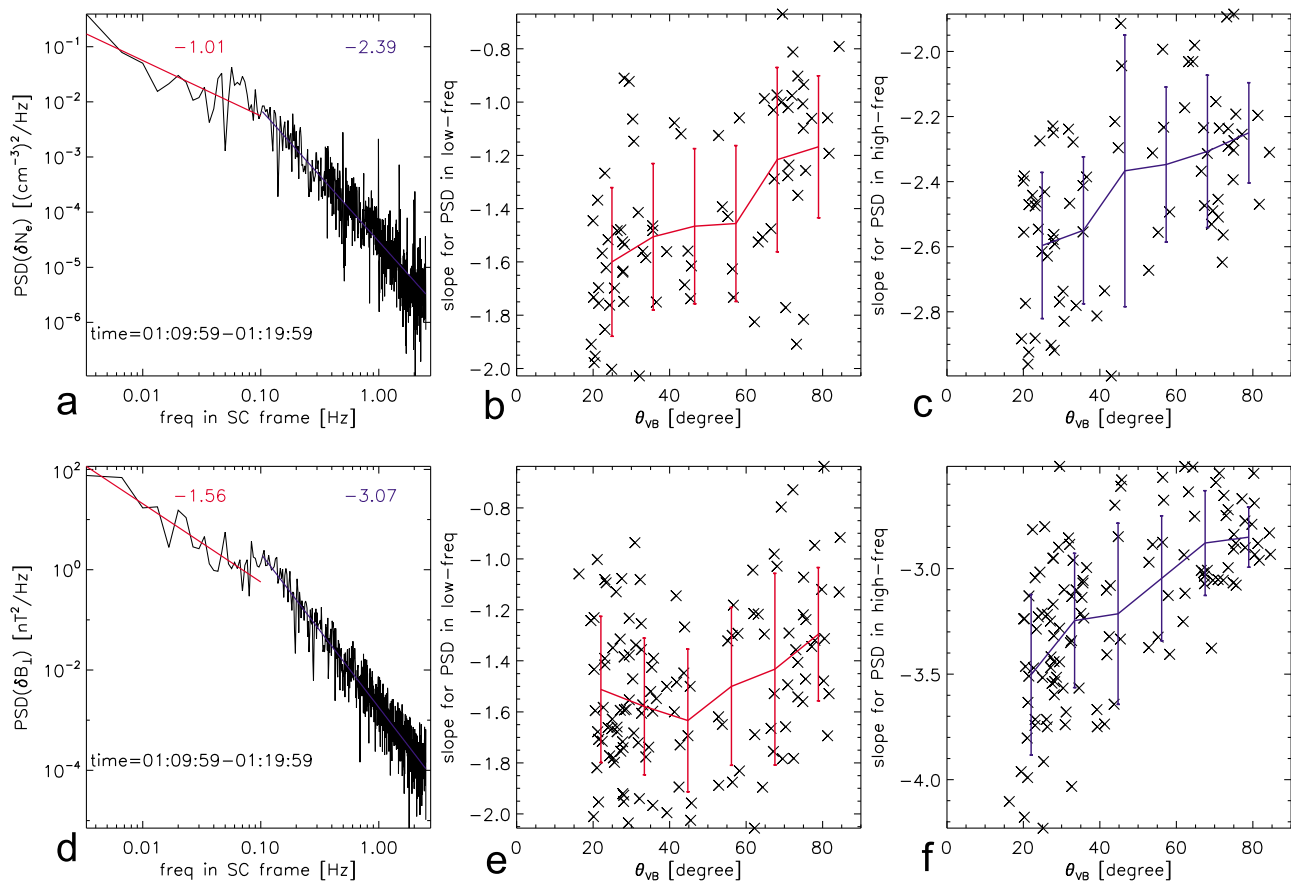
Figure 5. (a) PSD of number density fluctuations in the time interval [0110, 0120]. Power law fitting results for both the lower- and higher-frequency segments are shown as red and blue lines with their respective slopes marked as red and blue numbers. (b) Slopes of low-frequency PSD (δN_e) for different θ_{VB}. The red line and error bars represent the average and standard deviation, respectively, in every θ_{VB} bin. (c) Slopes of high-frequency PSD (δN_e) for different θ_{VB}. (d) PSD of $\delta B_\perp$ in the time interval [0110, 0120]. (e and f) Slopes of lower- and higher-frequency PSD ($\delta B_\perp$) for different θ_{VB}.

field fluctuations [*Lacombe and Belmont*, 1995]. In general, the 2-D SCFs revealed here sheds new light on the anisotropy of magnetosheath turbulence, and may also be relevant to other plasmas such as the solar wind and solar corona. In the future, to examine the development of turbulence in the magnetosheath downstream of the bow shock, the spatial evolution of the correlation function from the bow shock may be also needed to be studied besides the spatial tendency of intermittency investigated by *Yordanova et al.* [2008].

References

Alexandrova, O. (2008), Solar wind vs magnetosheath turbulence and Alfvén vortices, *Nonlinear Processes Geophys.*, *15*, 95.

Alexandrova, O., A. Mangeney, M. Maksimovic, N. Cornilleau-Wehrlin, J.-M. Bosqued, and M. André (2006), Alfvén vortex filaments observed in magnetosheath downstream of a quasi-perpendicular bow shock, *J. Geophys. Res.*, *111*, A12208, doi:10.1029/2006JA011934.

Alexandrova, O., C. Lacombe, and A. Mangeney (2008), Spectra and anisotropy of magnetic fluctuations in the Earth's magnetosheath: Cluster observations, *Ann. Geophys.*, *26*, 3585.

Balogh, A., et al. (2001), The Cluster magnetic field investigation: Overview of in-flight performance and initial results, *Ann. Geophys.*, *19*, 1207.

Bruno, R., and V. Carbone (2005), The solar wind as a turbulence laboratory, *Living Rev. Sol. Phys.*, *2*, 4.

Chen, C. H. K., T. S. Horbury, A. A. Schekochihin, R. T. Wicks, O. Alexandrova, and J. Mitchell (2010), Anisotropy of solar wind turbulence between ion and electron scales, *Phys. Rev. Lett.*, *104*, 255002, doi:10.1103/PhysRevLett.104.255002.

Décréau, P. M. E., et al. (1997), WHISPER, a resonance sounder and wave analyser: Performances and perspectives for the Cluster mission, *Space Sci. Rev.*, *79*, 157.

Escoubet, C. P., M. Fehringer, and M. Goldstein (2001), The Cluster mission, *Ann. Geophys.*, *19*, 1197.

Goldreich, P., and S. Sridhar (1995), Toward a theory of interstellar turbulence. II: Strong Alfvénic turbulence, *Astrophys. J.*, *438*, 763.

Goldstein, M. L., D. A. Roberts, and W. H. Matthaeus (1995), Magnetohydrodynamic turbulence in the solar wind, *Annu. Rev. Astron. Astrophys.*, *33*, 283.

Gustafsson, G., et al. (2001), First results of electric field and density observations by Cluster EFW based on initial months of operation, *Ann. Geophys.*, *19*, 1219.

Horbury, T. S. (2000), Cluster II analysis of turbulence using correlation functions, in *Cluster-II Workshop Multiscale/Multipoint Plasma Measurements*, edited by R. A. Harris, *Eur. Space Agency Spec. Publ.*, *ESA SP-449*, 89.

Horbury, T. S., M. Forman, and S. Oughton (2008), Anisotropic scaling of magnetohydrodynamic turbulence, *Phys. Rev. Lett.*, *101*, 175005, doi:10.1103/PhysRevLett.101.175005.

Kellogg, P. J., and T. S. Horbury (2005), Rapid density fluctuations in the solar wind, *Ann. Geophys.*, *23*, 3765.

Lacombe, C., and G. Belmont (1995), Waves in the Earth's magnetosheath: Observations and interpretations, *Adv. Space Res.*, *15*, 329.

Leamon, R. J., C. W. Smith, N. F. Ness, W. H. Matthaeus, and H. K. Wong (1998), Observational constraints on the dynamics of the interplanetary magnetic field dissipation range, *J. Geophys. Res.*, *103*, 4775.

Lucek, E. A., D. Constantinescu, M. L. Goldstein, J. Pickett, J. L. Pinçon, F. Sahraoui, R. A. Treumann, and S. N. Walker (2005), The magnetosheath, *Space Sci. Rev.*, *118*, 95.

Mangeney, A., C. Lacombe, M. Maksimovic, A. A. Samsonov, N. Cornilleau-Wehrlin, C. C. Harvey, J.-M. Bosqued, and P. Trávníček (2006), Cluster observations in the magnetosheath—Part 1: Anisotropies of the wave vector distribution of the turbulence at electron scales, *Ann. Geophys.*, *24*, 3507.

Marsch, E., and C.-Y. Tu (1990), Spectral and spatial evolution of compressible turbulence in the inner solar wind, *J. Geophys. Res.*, *95*, 11,945.

Matthaeus, W. H., M. L. Goldstein, and J. H. King (1986), An interplanetary magnetic field ensemble at 1 AU, *J. Geophys. Res.*, *91*, 59.

Matthaeus, W. H., M. L. Goldstein, and D. A. Roberts (1990), Evidence for the presence of quasi-two-dimensional nearly incompressible fluctuations in the solar wind, *J. Geophys. Res.*, *95*, 20,673.

Matthaeus, W. H., S. Dasso, J. M. Weygand, L. J. Milano, C. W. Smith, and M. G. Kivelson (2005), Spatial correlation of solar-wind turbulence from two-point measurements, *Phys. Rev. Lett.*, *95*, 231101, doi:10.1103/Phys/RevLett.95.231101.

Narita, Y., and K.-H. Glassmeier (2006), Propagation pattern of low frequency waves in the terrestrial magnetosheath, *Ann. Geophys.*, *24*, 2441.

Osman, K. T., and T. S. Horbury (2007), Multispacecraft measurement of anisotropic correlation functions in solar wind turbulence, *Astrophys. J.*, *654*, L103.

Pedersen, A., et al. (2008), Electron density estimations derived from spacecraft potential measurements on Cluster in tenuous plasma regions, *J. Geophys. Res.*, *113*, A07S33, doi:10.1029/2007JA012636.

Podesta, J. J. (2009), Dependence of solar-wind power spectra on the direction of the local mean magnetic field, *Astrophys. J.*, *698*, 986.

Rème, H., et al. (2001), First multispacecraft measurements in and near the Earth's magnetosphere with the identical Cluster ion spectrometry (CIS) experiment, *Ann. Geophys.*, *19*, 1303.

Sahraoui, F., G. Belmont, L. Rezeau, N. Cornilleau-Wehrlin, J. L. Pinçon, and A. Balogh (2006), Anisotropic turbulent spectra in the terrestrial magnetosheath as seen by the Cluster spacecraft, *Phys. Rev. Lett.*, *96*, 075002, doi:10.1103/PhysRevLett.96.075002.

Schekochihin, A. A., S. C. Cowley, W. Dorland, G. W. Hammett, G. G. Howes, E. Quataert, and T. Tatsuno (2009), Astrophysical gyrokinetics: Kinetic and fluid turbulent cascades in magnetized weakly collisional plasmas, *Astrophys. J., Suppl. Ser.*, *182*, 310.

Schwartz, S. J., D. Burgess, and J. J. Moses (1996), Low-frequency waves in the Earth's magnetosheath: Present status, *Ann. Geophys. (C. N. R. S.)*, *14*, 1134.

Tu, C.-Y., and E. Marsch (1995), MHD structures, waves and turbulence in the solar wind: Observations and theories, *Space Sci. Rev.*, *73*, 1.

Weygand, J. M., W. H. Matthaeus, S. Dasso, M. G. Kivelson, L. M. Kistler, and C. Mouikis (2009), Anisotropy of the Taylor scale and the correlation scale in plasma sheet and solar wind magnetic field fluctuations, *J. Geophys. Res.*, *114*, A07213, doi:10.1029/2008JA013766.

Yordanova, E., A. Vaivads, M. André, S. C. Buchert, and Z. Vörös (2008), Magnetosheath plasma turbulence and its spatiotemporal evolution as observed by the Cluster spacecraft, *Phys. Rev. Lett.*, *100*, 205003, doi:10.1103/PhysRevLett.100.205003.

J.-S. He, C.-Y. Tu, S. Yao, and Q.-G. Zong, Department of Geophysics, School of Earth and Space Sciences, Peking University, Beijing, 100871, China. (jshept@gmail.com)

E. Marsch, Max-Planck Institute for Solar System Research, D-37191 Katlenburg-Lindau, Germany.

H. Tian, National Center for Atmospheric Research, Boulder, CO 80301, USA.